

The highly polarized open cluster Trumpler 27¹

Carlos Feinstein², Gustavo Baume³, Ruben Vazquez², Virpi Niemela⁴

Observatorio Astronómico, Paseo del Bosque, B1900FWA La Plata, Argentina

and

Miguel Angel Cerruti²

Instituto de Astronomía y Física del Espacio, CC 67, Sucursal 28, 1428 Buenos Aires,
Argentina

Received _____; accepted _____

¹Based on observations obtained at Complejo Astronómico El Leoncito (CASLEO), operated under agreement between CONICET and the National Universities of La Plata, Córdoba, and San Juan, Argentina.

³On a fellowship from CONICET, Argentina.

²Member of Carrera del Investigador Científico, CONICET, Argentina.

⁴Member of Carrera del Investigador Científico, CIC, Prov. Buenos Aires, Argentina.

ABSTRACT

We have carried out multicolor linear polarimetry (UBVRI) of the brightest stars in the area of the open cluster Trumpler 27. Our data show a high level of polarization in the stellar light with a considerable dispersion, from $P = 4\%$ to $P = 9.5\%$. The polarization vectors of the cluster members appear to be aligned. Foreground polarization was estimated from the data of some non-member objects, for which two different components were resolved: the first one associated with a dust cloud close to the Sun producing $P_{\lambda max} = 1.3\%$ and $\theta = 146$ degrees, and a second component, the main source of polarization for the cluster members, originated in another dust cloud, which polarizes the light in the direction of $\theta = 29.5$ degrees. From a detailed analysis, we found that the two components have associated values $E_{B-V} < 0.45$ for the first one, and $E_{B-V} > 0.75$ for the other. Due the difference in the orientation of both polarization vectors, almost 90 degrees (180 degrees at the Stokes representation), the first cloud ($\theta \sim 146$ degrees) depolarize the light strongly polarized by the second one ($\theta \sim 29.5$ degrees).

Subject headings: **ISM: dust,extinction, open clusters and associations: individual (Trumpler 27)**

1. Introduction

Trumpler 27 ($l = 355$, $b = -0.7$), also known as C1732-334, is a heavily reddened open cluster located approximately in the direction to the galactic center. This cluster deserved a major attention in the past because some of its brightest members are stars that play a dominant role when trying to interpret the different evolutionary phases of the brightest massive stars. Tr 27-102 is a long period Cepheid (Van Genderen et al. 1978, Bakker et al. 1981). Tr 27-28 and Tr 27-105 are two known Wolf-Rayet stars (WR 95 and WR 98 respectively) in the catalogue of galactic WR stars (van der Hucht et al. 1981). The first of them has a very large infrared excess due to thermal re-emission of the stellar UV radiation by dust grains (Thé et al. 1980).

The literature reports three previous studies of the stellar population in Tr 27 with the main interest to determine the distance to the cluster, namely Thé and Stokes (1970); Moffat, FitzGerald & Jackson (1977, hereafter MFJ77); Bakker & Thé, (1983, hereafter BT83). This last study determined a distance of 1.65 ± 0.25 kpc using five color (WULBV) Walraven photometry, locating the Tr 27 cluster in the Sagittarius arm. MFJ77 found Tr 27 to be $6 \cdot 10^6$ year old cluster containing eight supergiants stars, six are blue (#2,8,23,43,46,46a), one is yellow (#102) and one is red (#1).

MFJ77 also argued due to the lack of detected $H\alpha$ emission or a reflection nebula that the layer of dust causing the strong reddening of the cluster ($E_{(B-V)} \sim 1.25$) is in front, but not associated with Tr 27. BT83 also found a normal extinction law analyzing 3 stars observed in several wavelengths and suggested that the radiation of these stars is already diluted when it reaches the dark cloud.

In order to understand the physical properties of the interstellar medium (ISM) towards Trumpler 27, we have carried out linear polarization observations of its brightest stars. In the next sections we will discuss the observational procedures, the data calibration and the

results in terms of both individual stars and the whole cluster.

2. Observations and data reduction

Data of linear polarimetry were obtained during three observing runs at the Complejo Astronómico El Leoncito (CASLEO) San Juan, Argentina, using two different photopolarimeters attached to the 2.15 m telescope. The first observations were performed using the Vatican Polarimeter (VATPOL) during June 11-15, 1991, while the rest were carried out with the Torino Five Channel Photopolarimeter in May 30-June 3, 1995 and June 30, 1997. Most of the stars were observed through the Johnson broad band UBVRI filters ($\lambda_{U_{eff}} = 0.360 \mu m$, $\lambda_{B_{eff}} = 0.440 \mu m$, $\lambda_{V_{eff}} = 0.530 \mu m$, $\lambda_{R_{eff}} = 0.690 \mu m$, $\lambda_{I_{eff}} = 0.830 \mu m$), but a few fainter ones were observed in white light, i.e. without any filter (VATPOL run only). Several polarization standard stars (for angle and zero point) were also measured for calibration purposes. In order to verify the lack of systematic differences between the observations performed with both instruments, we show in Fig 1a,b the results obtained for a set of stars observed with both polarimeters. Notice that the straight lines in these figures are not least squares fits but the 45 degrees slopes drawn as a reference. No systematic difference was detected between the VATPOL and the Torino Five Channel Polarimeter data, as can be seen from the excellent agreement, as well for the values of the polarization vectors, as for their respective angles.

Our results are listed in table 1 which shows, in self explanatory format, the stellar identification as given by MJF77, the average of the percentage of polarization (P), and the position angle of the electric vector (θ) observed through each filter, with their respective mean errors.

Several stars in the area have been observed by the Hipparcos astrometric satellite and

are included in the Hipparcos/Tycho Catalogue Data (#1,2,16,23,24,43,102,103 and 104). However, all these stars are so far away from the Sun that no useful parallax measures could be obtained. Although #24 is a non-member star in front of the cluster, it too has a meaningless parallax in Hipparcos data.

3. Results

We want to emphasize, as seen from data in Table 1, the presence of cluster stars having linear polarization values reaching 9%. As far as we know, such values are not very often measured in an open cluster. The only case reported in the literature having measurements of polarization greater than Tr 27, is M17 where Schultz et al. (1981) found values in excess of 20% for some stars.

In figure 2 we show the sky projection of the V band polarization for the observed stars in Tr 27. As a reference the dashed line is the galactic parallel $b = -0^\circ.8$. Note the alignment of the polarization vectors with the galactic plane. An evident feature in this figure is also that some stars with low polarization (near $\sim 1\%$) do not follow the general trend shown by most of the stars in Tr 27. These stars (#4,6,22,24 and 26) were considered non-members in earlier investigations and they are very probably located in front of the cluster and the dark cloud near the cluster (MFJ77, BT83).

Figure 3a presents the histogram of the angle distribution of the polarization vectors for the observed stars. The non-member stars are easily detected due to their different angle, appearing as an isolated group at ~ 146 degrees. These objects can be used to estimate the interstellar polarization component (IP) in front of Tr 27 and to subtract its contribution from the measures of the cluster stars. Averaging the value for non-members stars, we find that the IP component is $P_V = 1.32 \pm 0.02\%$ and $\theta_V = 146.6 \pm 5$ degrees. This angle is not

aligned with the galactic plane, but appears almost perpendicular, showing a perturbation in the local magnetic field of the Galaxy on the line of sight to the Tr 27 cluster. As we do not know the distances to these foreground stars we can not estimate the extent over which the dust is aligned in this angle. From the data in the Catalogue of linear polarization of Axon and Ellis (1976), the angle of the polarization vector in this direction seems to show a complex pattern not associated with the direction of the galactic plane in a large range of distances. In the photometry of MFJ77, most of these non-member objects have colors compatible with low mass main sequence stars.

Figure 3b shows the plot of the observed linear polarization vector P_V vs the polarization angle. In this figure the segregation between the members of Tr 27 and non-members becomes more obvious, as the cluster stars appear much more polarized. It is interesting to note that the non-member stars 4 and 6 ($\sim 2.5'$ to the W from stars #22,24,26) are $\sim 0.2\%$ more polarized than the other non-members (also the angle is 10 degrees lower), which means that probably the IP component is not fixed at the field and probably has a gradient (Fig 3b) like the one found in the Carina Nebula by Marraco et al. (1993). However, with only a few objects to determine the IP, a selection in distance can not be ruled out.

In Fig. 3a, the stars observed in Tr 27 cluster appear very close to ~ 30 degrees in polarization angle, and the data can be easily fitted with a Gaussian distribution. The dispersion of this fit is ~ 10 degrees, which is in the range of the values found by Waldhausen et al. (1999) for the open clusters NGC 6167, NGC 6193 and NGC 6204 in Ara OB1. One star in Tr 27 (#103) seems to be less polarized than the others. Star #103 is an isolated object located 1° to the West where the ISM has different properties. This star was not considered for the fitting of the Gaussian distribution.

We note that the direction of pointing of the foreground component (IP) is 146.6

degrees, which is at near 90 degrees to the cluster component (~ 29.5 degrees), so that the total effect is to depolarize the light crossing through the ISM that produces the IP. Thus, the polarization percentages corrected for IP would be even larger than the observed ones.

BT83 suggested that the star #105 (WR 98) is a background object. However, our data indicate that the light of this star has polarimetric properties ($P_V = 5.2 \pm 0.04\%$, $\theta = 49.1 \pm 0.2$ degrees) similar to the cluster members, because of the high polarization and the polarization angle average ($\theta \sim 30 \pm 10$ degrees). As this star is a Wolf-Rayet type binary system (Niemela 1999) an intrinsic polarization component may be expected, but it would be hard to distinguish from the high value of the polarization of the ISM. We consider WR98 to be a probable member of the Tr 27 cluster.

4. Analysis and Discussion

To analyze the data, the polarimetric observations were fitted using the Serkowski law of interstellar polarization (Serkowski 1973). This is:

$$P_\lambda / P_{\lambda_{max}} = e^{-K \ln^2(\lambda_{max} / \lambda)} \quad [1]$$

If the polarization is produced by aligned interstellar dust particles, the observed data (in terms of wavelength, UBVRI) will follow [1], where each star is characterized by a $P_{\lambda_{max}}$ and a λ_{max} .

Adopting $K = 1.66\lambda_{max} + 0.01$ (Whittet et al., 1992), we fitted our observations and computed the σ_1 parameter (the unit weight error of the fit) in order to quantify the departure of our data from the “theoretical curve” of Serkowski’s law. A σ_1 larger than 1.5 is considered as an indication of the presence of a component of intrinsic stellar polarization. Another criterion of intrinsic stellar polarization is to compute the dispersion of position angle for each star normalized by the average of the position angle errors ($\bar{\epsilon}$).

The λ_{max} values can also be used to test the origin of the polarization. In fact, since the average value of λ_{max} for the interstellar medium is $0.545 \mu m$ (Serkowski et al. 1975), objects showing λ_{max} rather lower than this value are also candidates for having an intrinsic component of polarization (e.g. Orsatti et al. 1998). The values that we have obtained for P , the σ_1 parameter, λ_{max} , and $\bar{\epsilon}$ together with the identification of stars are listed in Table 2.

Figure 4 shows the observed P and θ of those stars which are the candidates for having an intrinsic component of polarization. For purposes of comparison, the best fit to a Serkowski's law to these observations is also plot as a continuous line. Stars #1 and #2 (spectral types M0Ia and O9Ia, respectively, MFJ77) have a large departure of the Serkowski's relation for the data at the wavelengths of the I filter. Star #1 also shows a significant rotation in the position angle of the polarization vector. Both cases are noticeable despite the high polarization vector component added by the the dust, meaning a considerable intrinsic component of polarization. Stars #25 and #106 do not fit the Serkowski curve at U and I filters wavelengths.

The histogram of all the observed λ_{max} shown in Fig. 5 confirms that the most probable value of λ_{max} for stars in Tr27 is around $0.55 m\mu$, which is the same value found by Serkowski et al (1975) as the average value for the ISM.

The observed polarization $P(\%)$ and θ of the non-member stars show that there exist dust particles in a different alignment than those observed in the highly polarized light of the Tr 27 cluster stars. We ill try to estimate the effect of this layer of dust particles, characterizing its properties ($P(\%)$, θ , E_{B-V} , etc). The polarization vector and the angle of orientation can be obtained from the non-members stars #4,6,20,22 and 24, which give by fitting a Serkowski law to each one of these stars an average of $P_{\lambda_{max}} = 1.35$ and $\theta = 146.6$.

Figure 6 is the plot of the $P_{\lambda_{max}}$ (corrected by the IP vector) vs E_{B-V} (data

from MFJ77), but not corrected for E_{B-V} of the IP, because the value is unknown. The dashed line is the empirical upper limit relation for the interstellar polarization, $P_{\lambda max} = R A_v \sim 9E_{B-V}$ (for normal dust, $R = 3.2$), Serkowski et al. (1975). If we consider that the star #23 is nearly the case of the maximum observed efficiency for the dust to polarize light, we can shift the dashed line over the E_{B-V} axis up to the location of star #23 (the solid line in Fig. 6). This displacement ($\Delta E_{B-V} = 0.45$) then represents the maximum E_{B-V} allowed for the IP component ($E_{B-V IP}$). Note, that if the slope of the relation $P_{\lambda max}$ vs E_{B-V} is lower than 9, as it probably is, the maximum value of E_{B-V} for the IP component will decrease. Therefore, we can conclude that the IP component at least must have an $E_{B-V IP} \leq 0.45$

MFJ77 and BT83 have confirmed that the total mean color excess towards Trumpler 27 is $E_{B-V} = 1.2$. As we found that $E_{B-V IP} \leq 0.45$, the cloud that causes the high polarization must be associated with $E_{B-V} > 0.75$ (second component). Also both above mentioned papers argue that this last layer of dust (the second component) must be in front but not associated with the Tr 27 cluster due to the lack of $H\alpha$ emission or a reflection nebula (MFJ77); and since the extinction law appears normal for 3 luminous stars the radiation of these stars is already diluted when it reaches the dark cloud (BT83). On the other hand, in both papers their two-color plots show a wide dispersion and not a sharp sequence, implying that some of this dust may be intracluster or just in front of the cluster, but with a density distribution that appears very non-homogeneous.

Using the MFJ77 data for the non-member stars, and considering the value $E_{B-V IP} < 0.45$, we find that some of these objects are consistent with solar type main sequence stars. To achieve the average polarization $P_{\lambda max} = 1.35$ for normal efficiency of the polarizing properties of the dust ($P_{\lambda max}/E_{B-V} \sim 5$, Serkowski et al., 1975) the $E_{B-V IP}$ can not be larger than $E_{B-V IP} \sim 0.3$, which is still in the range of $E_{B-V IP} \leq 0.45$.

Excluding the cluster stars with the highest polarization percentage, namely #23,25 and 27 and also the star #103 with the lower polarization, the rest of the Tr 27 stars seems to be aligned in Fig. 6. The slope of this alignment is the polarization efficiency of the ISM. The fit for these stars gives $P_{\lambda max}/E_{B-V} = 4.6 \pm 0.12$, which is similar to the value of $P_{\lambda max}/E_{B-V} = 5$ mentioned above as the canonical value for ISM.

This picture of two dust components agrees with the behavior of the interstellar absorption in this direction of the galaxy according the study of the spatial distribution of the interstellar dust by Neckel & Klare (1980). Their work shows a strong jump in absorption from 1 *mag* to 4 *mag* at about 1 Kpc.

5. Conclusions

We have observed linear polarization (P and θ) for a sample of stars in the open cluster Trumpler 27, and also a few non-member objects. Our observations indicate that the cluster members show a percentage of polarization up to 9%, an unusually high value for an open clusters. The dispersion of polarization values goes from 4 to 9%, while the average orientation of polarization is 29.5 degrees, with a dispersion of 10 degrees approximately.

Using the non-member stars, located in front of the cluster, we could identify a first component of interstellar polarization (IP), which is characterize by $P_V = 1.32 \pm 0.02$ and a mean polarization angle of $\theta_V = 146.6 \pm 5$ degrees. The second component that accounts for the bulk of the high polarization properties in Trumpler 27, has a mean polarization angle of $\theta_V = 29.5$ degrees, oriented along the galactic plane.

From the analysis of the relation between extinction and polarization it is possible to estimate the extinction related with each dust cloud component. For the group of non-member stars, we found $E_{B-V} < 0.45$, a value which is in good agreement with previous

photometric values. The second component must have an $E_{B-V} > 0.8$ to account for the previous photometry (MFJ77 , BT83).

We wish to acknowledge the technical support of CASLEO during our observing runs. We thank the Vatican Observatory for the loan of their polarimeter. Also we want to acknowledge useful discussions with Ana M. Orsatti, Nidia Morrell and Hugo Marraco, which are greatly appreciated.

REFERENCES

Axon, D.J., Ellis, R.S. 1976, MNRAS, 177,499

Bakker, R., Genderen, A.M. van 1981, IAU Inform. Bull. 1409, IAU Commision 27.

Bakker, R., Thé, P.S. 1983, A&AS, 52, 27 (BT 83)

van Genderen, A.M., Thé, P.S. 1978, A&A, 64,11

van der Hucht, K. A., Conti, P. S., Lundstrom, I., Stenholm, B. 1981, Space Science Reviews, 28,227

Marraco, H.G., Vega, E.I., Vrba, F.J. 1993, AJ 105,258

Moffat, A.F.J., FitzGerald, M.P., Jackson, P.D. 1977, AJ 87, 695 (MFJ77)

Neckel, T.H., Klare, G. 1980, A&AS 42,251

Niemela, V.S. 1991, in Proc. IAU Symp. 143, van der Hucht, K.A. and Hidayat, B. (eds) Kluwer-Dordrecht, 201

Schulz, A., Lenzen, R., Schmidt, Th., Proetel, K. 1981, A&A 95,94

Serkoswki, S. 1973, in Proc IAU Symposium N 52, Greenberg, J.M. and van den Hulst, H.C., (eds). Interstellar Dust and Related topics, Reidel, Dordrecht-Holland, p. 144

Serkowski, K., Mathewson, D. L., Ford, V. L. 1975, ApJ 196,261

Thé, P.S., Stokes, N. 1970, å 5, 298

Thé, P.S., Tjin A Djie, H.R.E., Wamsteker, W. 1980, A&A 84,263

Waldhausen, S., Martínez R., Feinstein, C. 1999, AJ 117,2882

Whittet, D.C.B., Martin, P.G., Hough, J.H., Rouse, M.F., Nailey, J.A., Axon, D.J. 1992, ApJ 386, 562

Fig. 1.— Comparison of the data for the stars observed with both polarimeters

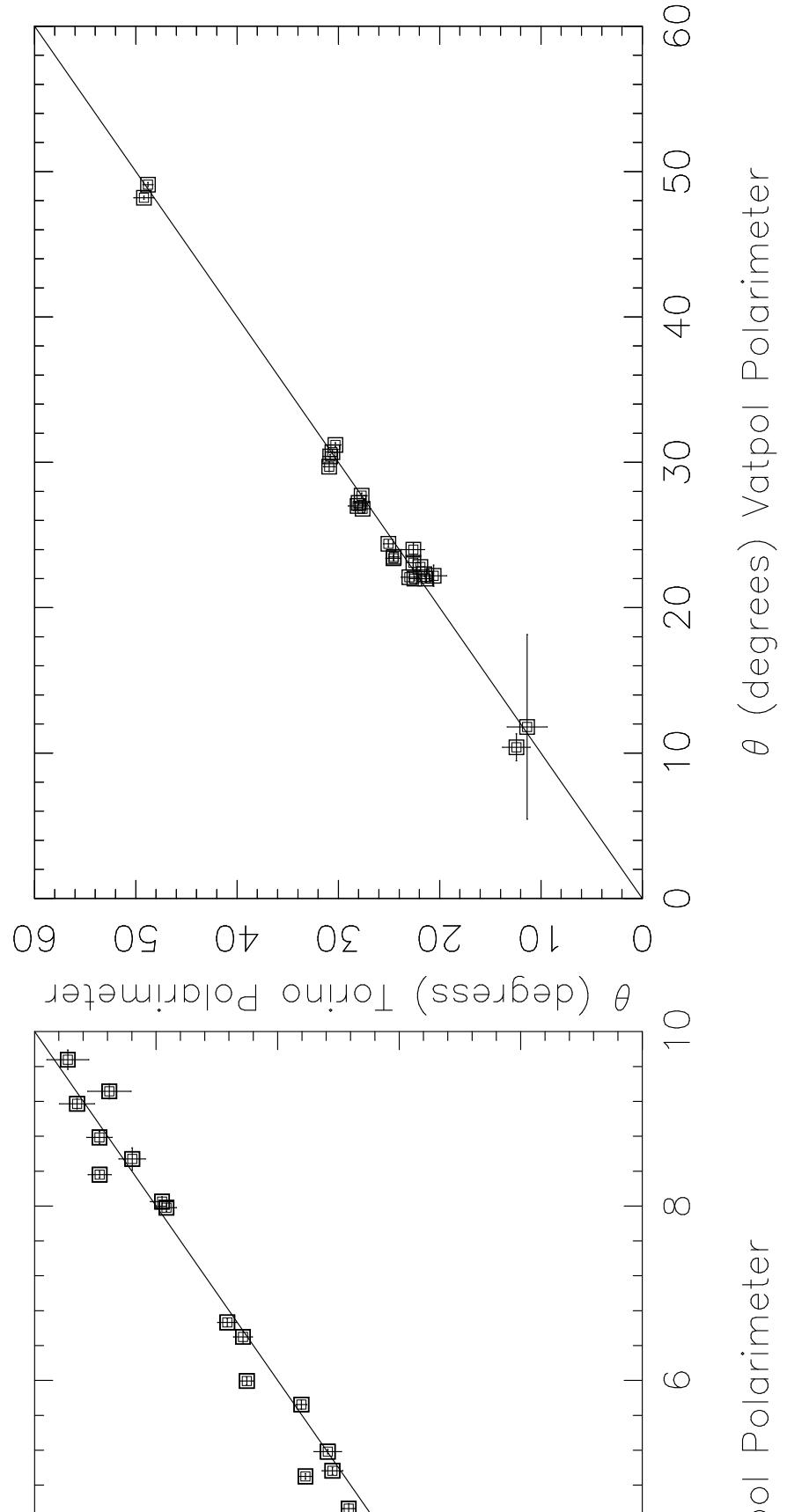


Fig. 2.— Projection of the polarization vectors (Johnson V filter) over the sky. The dotted line is the galactic parallel $b = -0^\circ.8$

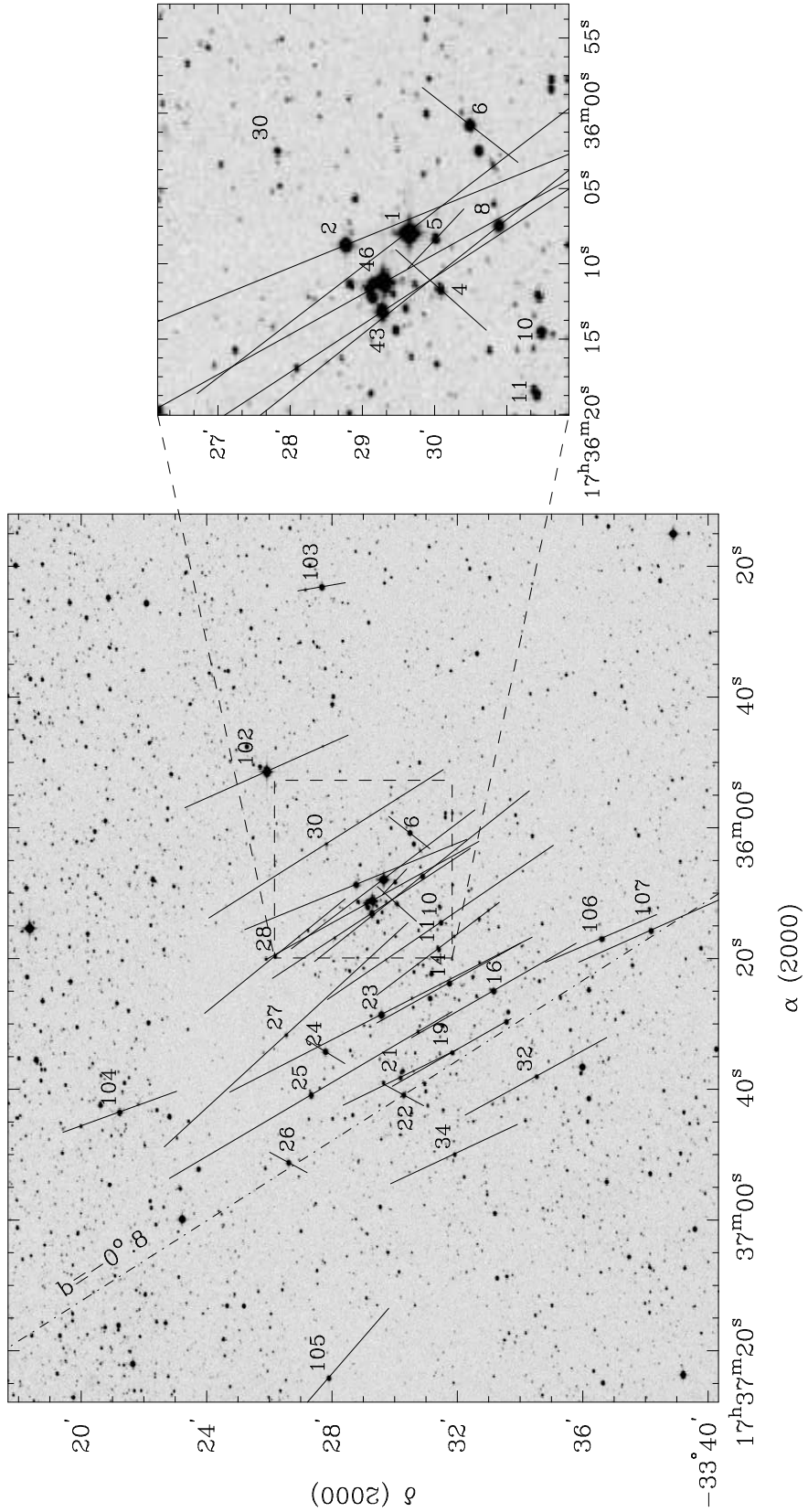


Fig. 3.— Top: Histogram of the polarization angle (θ) for the observed stars. Shadowed bars are for the Tr 27 cluster stars and white bars are for the foreground stars. The continuous line is the Gaussian fit to the data for members of Tr 27. Bottom: Polarization percentage of the stellar flux versus the polarization angle for each star. Note how the cluster stars and the non-member objects are segregated.

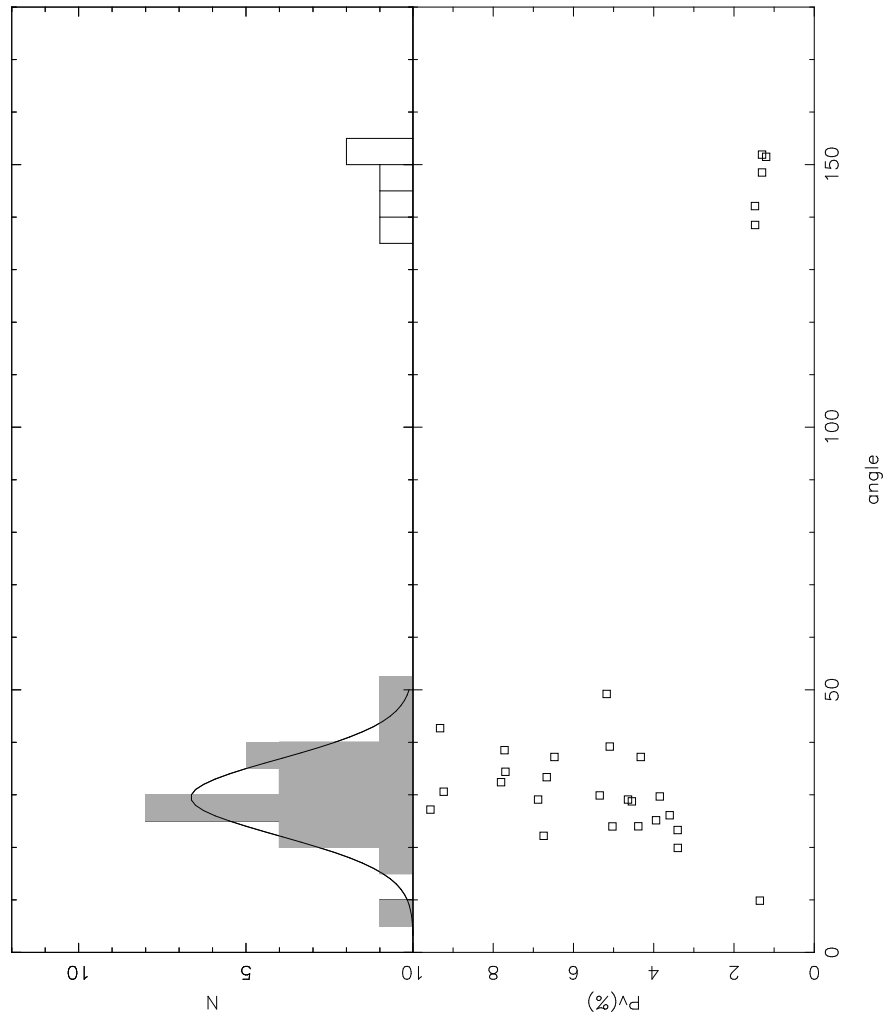


Fig. 4.— Plot of the observed data for objects showing large departures from the Serkowski law, the solid line is the best fit.

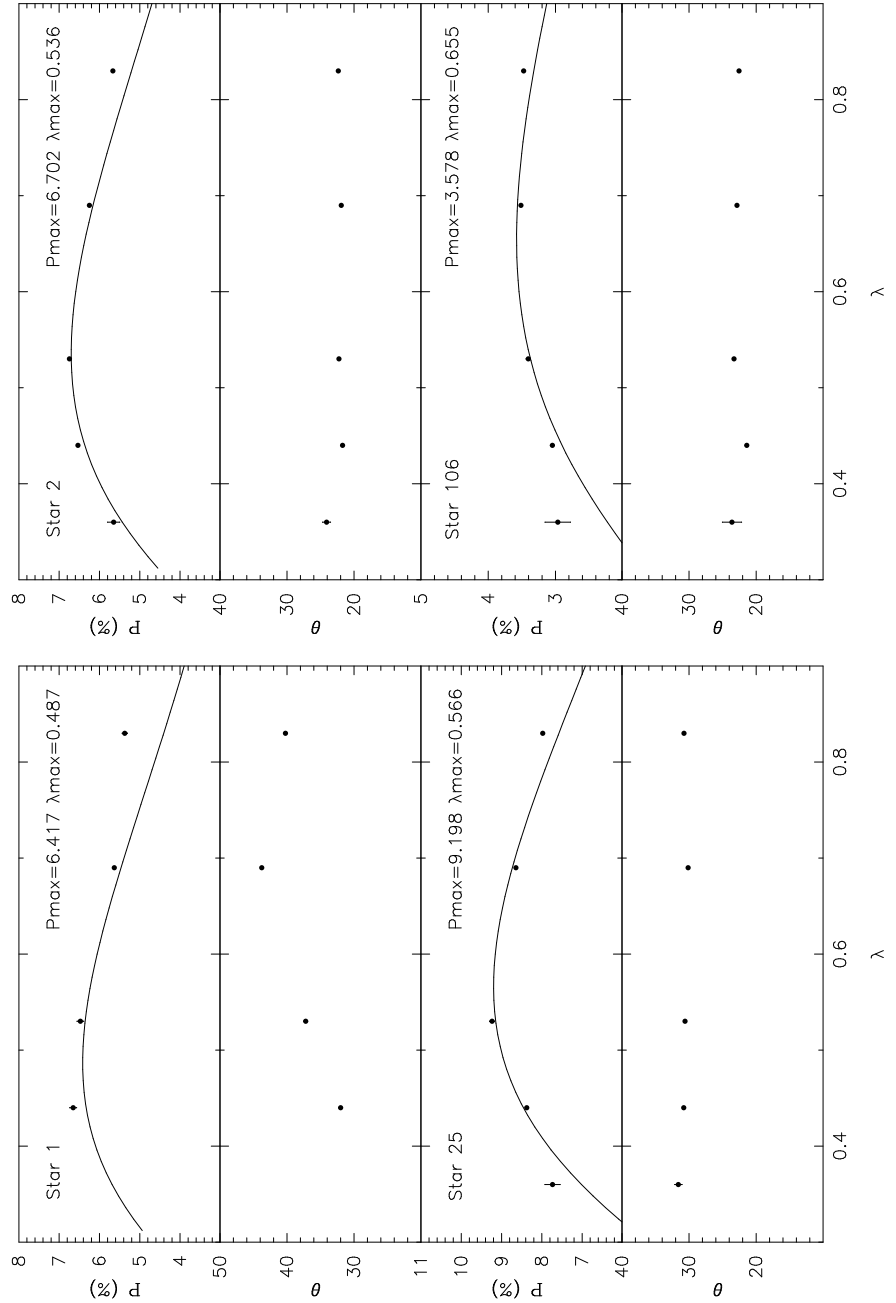


Fig. 5.— Histogram of the parameter λ_{max} obtained fitting the Serkowski law to the observations.

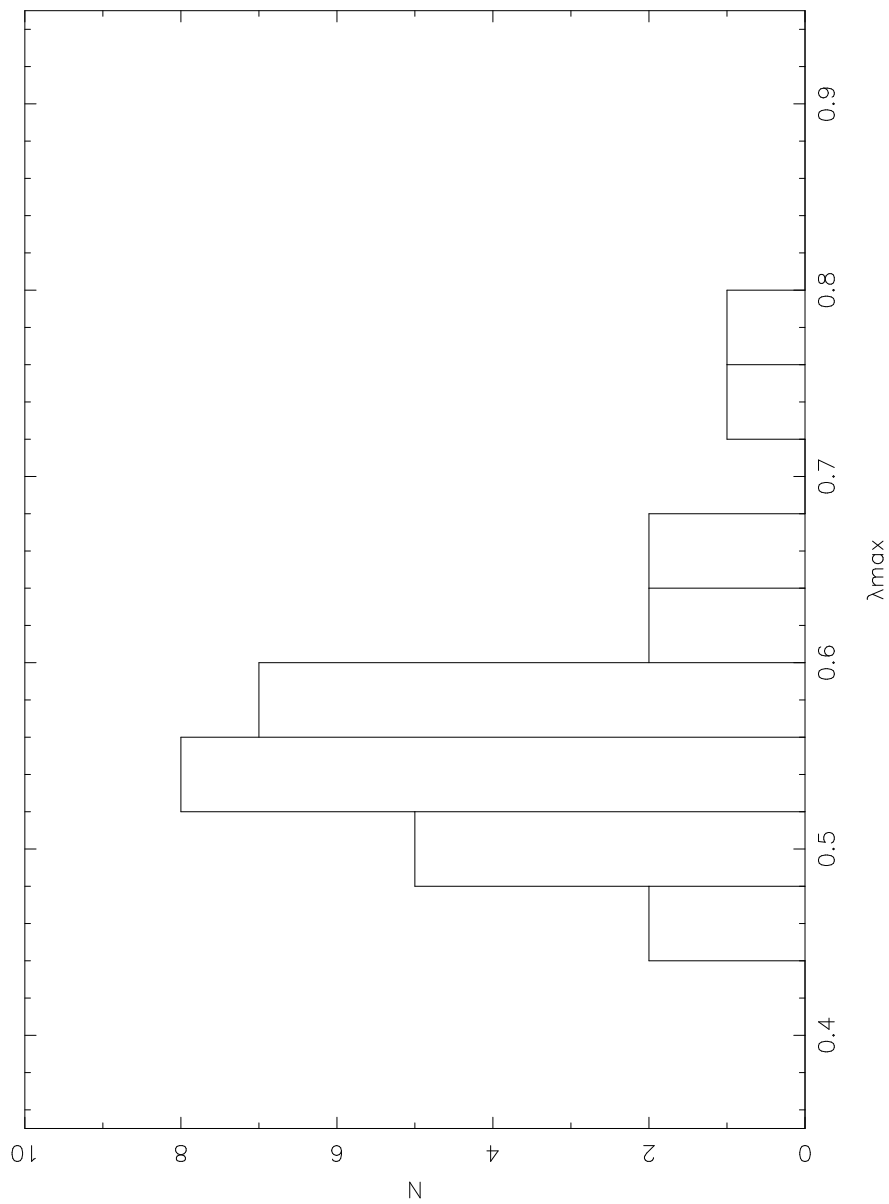


Fig. 6.— $P_{\lambda max}$ vs E_{B-V} . The dashed line is $P_{\lambda max} = 9E_{B-V}$, and the solid line is a parallel for an IP component of $E_{B-V} = 0.45$

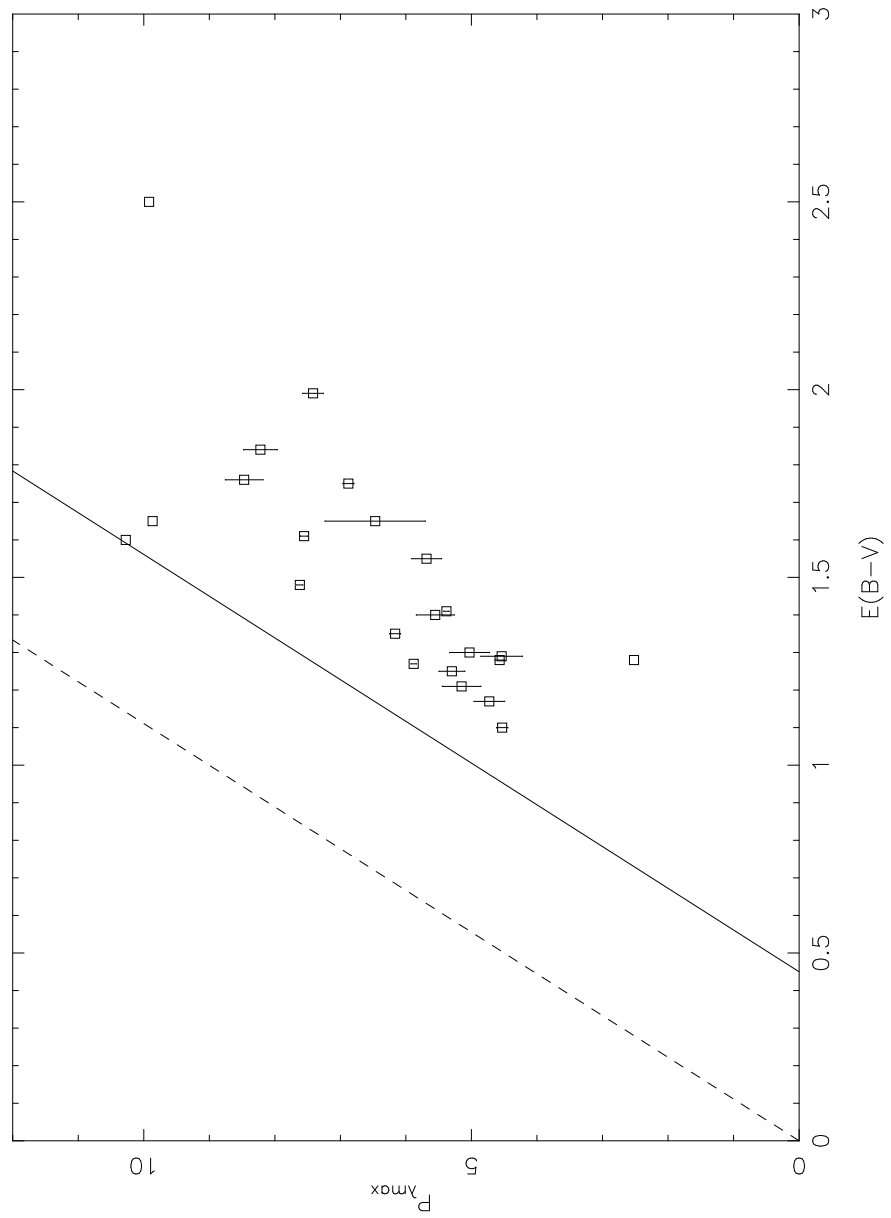


Table 1. Polarimetric Observations of stars in Tr 27

Filter	$P_\lambda \pm \epsilon_P$ %	$\theta_\lambda \pm \epsilon_\theta$ (deg)
Star 1		
B	6.65 \pm 0.09	32.0 \pm 0.4
V	6.47 \pm 0.08	37.2 \pm 0.4
R	5.63 \pm 0.03	43.8 \pm 0.1
I	5.37 \pm 0.07	40.2 \pm 0.4
Star 2		
U	5.65 \pm 0.15	24.1 \pm 0.8
B	6.53 \pm 0.02	21.7 \pm 0.1
V	6.75 \pm 0.02	22.2 \pm 0.1
R	6.25 \pm 0.01	21.9 \pm 0.1
I	5.67 \pm 0.01	22.4 \pm 0.1
Star 4		
B	1.04 \pm 0.26	146.4 \pm 6.9
V	1.48 \pm 0.20	138.5 \pm 3.8
R	1.47 \pm 0.15	140.1 \pm 2.9
I	1.55 \pm 0.29	125.5 \pm 5.4
Star 5		
U	4.18 \pm 0.62	38.8 \pm 4.2
B	1.63 \pm 0.66	60.8 \pm 11.1
V	1.00 \pm 0.76	46.8 \pm 18.7
Star 6		
B	1.80 \pm 0.28	140.3 \pm 4.3
V	1.48 \pm 0.08	142.1 \pm 1.6

Table 1—Continued

Filter	$P_\lambda \pm \epsilon_P$ %	$\theta_\lambda \pm \epsilon_\theta$ (deg)
R	1.51 \pm 0.08	142.2 \pm 1.4
I	1.18 \pm 0.13	140.9 \pm 3.1
Star 8		
U	7.32 \pm 0.57	37.3 \pm 2.2
B	6.74 \pm 0.40	38.3 \pm 1.7
V	7.72 \pm 0.26	38.5 \pm 1.0
R	7.16 \pm 0.18	41.2 \pm 0.7
I	6.32 \pm 0.17	41.6 \pm 0.8
Star 10		
U	7.28 \pm 0.65	30.3 \pm 2.5
B	8.05 \pm 0.44	32.7 \pm 1.6
V	7.70 \pm 0.29	34.4 \pm 1.1
R	6.79 \pm 0.17	33.8 \pm 0.7
I	5.85 \pm 0.15	35.5 \pm 0.7
Star 11		
U	3.06 \pm 0.35	33.5 \pm 3.3
B	3.73 \pm 0.29	36.2 \pm 2.2
V	4.32 \pm 0.29	37.2 \pm 1.9
R	4.58 \pm 0.15	37.6 \pm 0.9
I	4.21 \pm 0.16	40.3 \pm 1.1
Star 14		
V	4.64 \pm 0.04	29.1 \pm 0.3
R	4.24 \pm 0.05	29.3 \pm 0.4

Table 1—Continued

Filter	$P_\lambda \pm \epsilon_P$ %	$\theta_\lambda \pm \epsilon_\theta$ (deg)
I	4.05 ± 0.05	29.7 ± 0.4
Star 16		
U	4.10 ± 0.19	26.9 ± 1.3
B	5.06 ± 0.01	28.7 ± 0.1
V	5.35 ± 0.02	29.9 ± 0.1
R	5.22 ± 0.02	31.4 ± 0.1
I	4.72 ± 0.01	31.3 ± 0.1
Star 19		
U	3.28 ± 0.48	26.7 ± 4.1
B	3.51 ± 0.37	27.9 ± 3.0
V	3.85 ± 0.32	29.7 ± 2.4
R	3.44 ± 0.18	30.2 ± 1.5
I	2.62 ± 0.21	33.9 ± 2.3
Star 21		
U	3.47 ± 0.65	26.0 ± 5.3
B	3.40 ± 0.48	25.3 ± 4.1
V	3.58 ± 0.38	26.6 ± 3.0
R	3.77 ± 0.16	26.2 ± 1.2
I	3.00 ± 0.23	25.6 ± 2.2
Star 22		
U	1.94 ± 0.55	150.7 ± 7.8
B	1.23 ± 0.28	143.7 ± 6.3
V	1.30 ± 0.08	151.9 ± 1.6

Table 1—Continued

Filter	$P_\lambda \pm \epsilon_P$	$\theta_\lambda \pm \epsilon_\theta$
	%	(deg)
R	1.31 \pm 0.07	150.1 \pm 1.6
I	1.02 \pm 0.15	144.4 \pm 4.1
Star 23		
U	8.03 \pm 0.64	26.5 \pm 2.3
B	9.04 \pm 0.10	27.5 \pm 0.3
V	9.56 \pm 0.09	27.2 \pm 0.3
R	8.86 \pm 0.03	27.7 \pm 0.1
I	7.91 \pm 0.02	27.6 \pm 0.1
Star 24		
U	1.10 \pm 0.16	152.0 \pm 4.1
B	1.21 \pm 0.11	147.9 \pm 2.6
V	1.32 \pm 0.10	148.5 \pm 2.1
R	1.32 \pm 0.07	150.4 \pm 1.5
I	1.15 \pm 0.09	148.7 \pm 2.2
Star 25		
U	7.74 \pm 0.19	31.6 \pm 0.7
B	8.38 \pm 0.03	30.8 \pm 0.1
V	9.24 \pm 0.06	30.6 \pm 0.2
R	8.64 \pm 0.03	30.1 \pm 0.1
I	7.98 \pm 0.03	30.8 \pm 0.1
Star 26		
V	1.20 \pm 0.07	151.5 \pm 1.7
Star 27		

Table 1—Continued

Filter	$P_\lambda \pm \epsilon_P$	$\theta_\lambda \pm \epsilon_\theta$
	%	(deg)
B	7.71 \pm 0.95	45.4 \pm 3.5
V	9.32 \pm 0.41	42.7 \pm 1.3
R	9.31 \pm 0.18	42.8 \pm 0.6
I	8.07 \pm 0.24	42.6 \pm 0.8
Star 28		
U	4.06 \pm 1.54	68.4 \pm 10.4
B	4.24 \pm 1.01	29.5 \pm 6.7
V	5.10 \pm 0.76	39.2 \pm 4.3
R	5.39 \pm 0.24	35.3 \pm 1.3
I	4.84 \pm 0.17	35.2 \pm 1.0
Star 30		
U	6.92 \pm 1.35	24.4 \pm 5.5
B	7.77 \pm 0.80	33.3 \pm 2.9
V	7.80 \pm 0.55	32.4 \pm 2.0
R	7.23 \pm 0.22	34.6 \pm 0.9
I	6.50 \pm 0.34	35.3 \pm 1.5
Star 32		
U	4.26 \pm 0.36	27.0 \pm 2.4
B	4.53 \pm 0.38	28.0 \pm 2.4
V	4.54 \pm 0.30	28.8 \pm 1.9
R	4.63 \pm 0.12	29.2 \pm 0.7
I	3.64 \pm 0.19	28.8 \pm 1.5
Star 34		

Table 1—Continued

Filter	$P_\lambda \pm \epsilon_P$	$\theta_\lambda \pm \epsilon_\theta$
	%	(deg)
U	3.21 ± 0.41	23.8 ± 3.6
B	4.09 ± 0.47	27.7 ± 3.2
V	3.94 ± 0.30	25.2 ± 2.2
R	4.07 ± 0.14	25.0 ± 1.0
I	3.70 ± 0.27	25.0 ± 2.1
Star 43		
U	5.79 ± 0.31	36.2 ± 1.5
B	6.55 ± 0.15	34.0 ± 0.6
V	6.67 ± 0.16	33.4 ± 0.7
R	6.21 ± 0.15	35.3 ± 0.7
I	5.47 ± 0.13	35.1 ± 0.7
Star 46		
B	6.59 ± 0.05	28.9 ± 0.2
V	6.88 ± 0.06	29.1 ± 0.2
R	6.23 ± 0.05	29.8 ± 0.2
Star 102		
U	5.51 ± 0.59	26.5 ± 3.1
B	5.00 ± 0.29	23.0 ± 1.7
V	5.03 ± 0.02	24.0 ± 0.1
R	4.68 ± 0.01	24.0 ± 0.1
I	4.18 ± 0.01	24.7 ± 0.1
Star 103		
U	1.06 ± 0.22	11.9 ± 5.9

Table 1—Continued

Filter	$P_\lambda \pm \epsilon_P$	$\theta_\lambda \pm \epsilon_\theta$
	%	(deg)
B	1.181 \pm 0.08	11.3 \pm 0.1
V	1.36 \pm 0.06	9.9 \pm 1.2
R	1.82 \pm 0.00	11.4 \pm 0.1
I	1.28 \pm 0.11	11.6 \pm 2.5
Star 104		
U	2.86 \pm 0.12	20.4 \pm 1.2
B	3.33 \pm 0.12	18.1 \pm 1.0
V	3.40 \pm 0.09	19.9 \pm 0.7
R	3.51 \pm 0.08	19.1 \pm 0.6
I	3.13 \pm 0.07	19.8 \pm 0.6
Star 105		
U	4.50 \pm 0.47	53.5 \pm 3.0
B	4.82 \pm 0.04	51.2 \pm 0.3
V	5.20 \pm 0.04	49.1 \pm 0.2
R	5.20 \pm 0.01	48.9 \pm 0.1
I	4.88 \pm 0.02	48.4 \pm 0.1
Star 106		
U	2.97 \pm 0.19	23.6 \pm 1.8
B	3.05 \pm 0.03	21.4 \pm 0.3
V	3.40 \pm 0.03	23.3 \pm 0.3
R	3.51 \pm 0.01	22.9 \pm 0.1
I	3.47 \pm 0.02	22.5 \pm 0.2
Star 107		

Table 1—Continued

Filter	$P_\lambda \pm \epsilon_P$ %	$\theta_\lambda \pm \epsilon_\theta$ (deg)
U	3.71 ± 0.19	24.2 ± 1.5
B	3.98 ± 0.18	23.4 ± 1.3
V	4.39 ± 0.20	24.0 ± 1.3
R	4.24 ± 0.13	24.1 ± 0.9
I	3.75 ± 0.18	23.7 ± 1.4

Table 3. Parameters of the Serkowski fit to the linear polarization data for stars in Tr 27

Stellar Identification	$P_{max} \pm \epsilon_P$ %	σ_1	$\lambda_{max} \pm \epsilon_{\lambda_{max}}$ m μ	$\bar{\epsilon}$
1	6.417 ± 0.367	5.862	0.487 ± 0.044	48.08
2	6.702 ± 0.058	5.078	0.536 ± 0.007	0.30
4	1.529 ± 0.108	0.570	0.727 ± 0.098	6.53
6	1.551 ± 0.102	1.257	0.518 ± 0.070	0.11
8	7.605 ± 0.194	1.186	0.529 ± 0.023	1.71
10	7.883 ± 0.115	0.433	0.441 ± 0.009	1.01
11	4.528 ± 0.057	0.326	0.656 ± 0.018	1.55
14	4.608 ± 0.133	3.448	0.551 ± 0.036	0.17
16	5.372 ± 0.012	1.278	0.570 ± 0.002	4.44
19	3.725 ± 0.194	0.874	0.470 ± 0.034	1.51
21	3.821 ± 0.196	0.980	0.530 ± 0.048	0.04
22	1.343 ± 0.069	1.057	0.524 ± 0.062	1.09
23	9.417 ± 0.047	1.038	0.534 ± 0.004	0.02
24	1.336 ± 0.017	0.335	0.579 ± 0.013	0.54
25	9.038 ± 0.075	3.961	0.576 ± 0.009	0.40
27	9.430 ± 0.351	1.327	0.567 ± 0.045	0.07
28	5.347 ± 0.102	0.453	0.620 ± 0.022	1.49
30	7.799 ± 0.073	0.213	0.522 ± 0.008	0.86
32	4.814 ± 0.204	1.334	0.512 ± 0.036	0.19
34	4.122 ± 0.057	0.470	0.595 ± 0.019	0.21
43	6.673 ± 0.026	0.289	0.519 ± 0.004	0.83
46	6.777 ± 0.066	2.158	0.513 ± 0.013	0.73
102	4.999 ± 0.030	1.749	0.530 ± 0.005	0.13

Table 3—Continued

Stellar Identification	$P_{max} \pm \epsilon_P$	σ_1	$\lambda_{max} \pm \epsilon_{\lambda_{max}}$	$\bar{\epsilon}$ $m\mu$
103	1.844 ± 0.170	3.265	0.776 ± 0.078	0.01
104	3.520 ± 0.036	0.880	0.585 ± 0.012	0.47
105	5.269 ± 0.014	1.337	0.612 ± 0.006	0.12
106	3.578 ± 0.046	3.826	0.655 ± 0.020	0.41
107	4.354 ± 0.047	0.570	0.562 ± 0.012	0.06